# Aerodynamic design of an electronics pod to maximise its carriage envelope on a fast-jet aircraft

*Ruan du Rand*
Mechanical and Aeronautical Engineering Department, University of Pretoria, Pretoria, South Africa
*Kevin Jamison*
Aeronautic Systems Impact Area, Council for Scientific and Industrial Research, Pretoria, South Africa, and
*Barbara Huyssen*
Mechanical and Aeronautical Engineering Department, University of Pretoria, Pretoria, South Africa

## Abstract

**Purpose** – The purpose of this paper is to reshape a fast-jet electronics pod's external geometry to ensure compliance with aircraft pylon load limits across its carriage envelope while adhering to onboard system constraints and fitment specifications.

**Design/methodology/approach** – Initial geometric layout determination used empirical methods. Performance approximation on the aircraft with added fairings and stabilising fin configurations was conducted using a panel code. Verification of loads was done using a full steady Reynolds-averaged Navier–Stokes solver, validated against published wind tunnel test data. Acceptable load envelope for the aircraft pylon was defined using two already-certified stores with known flight envelopes.

**Findings** – Re-lofting the pod's geometry enabled meeting all geometric and pylon load constraints. However, due to the pod's large size, re-lofting alone was not adequate to respect aircraft/pylon load limitations. A flight restriction was imposed on the aircraft's roll rate to reduce yaw and roll moments within allowable limits.

**Practical implications** – The geometry of an electronics pod was redesigned to maximise the permissible flight envelope on its carriage aircraft while respecting the safe carriage load limits determined for its store pylon. Aircraft carriage load constraints must be determined upfront when considering the design of fast-jet electronic pods.

**Originality/value** – A process for determining the unknown load constraints of a carriage aircraft by analogy is presented, along with the process of tailoring the geometry of an electronics pod to respect aerodynamic load and geometric constraints.

**Keywords** Electronics pod, Aircraft store integration, Carriage loads, Integration by analogy, Computational analysis

**Paper type** Case study

## Nomenclature

### Symbols

$\alpha$ = angle of attack (°);
$\beta$ = sideslip angle (°);
Cp = coefficient of pressure (−);
$C_{Mx,y,z}$ = moment coefficient x,y or z (−);
$C_x$ = axial force coefficient (−);
$\rho$ = density (kg/m$^3$);
Q = volume flow rate (m$^3$/s);
A = channel area (m$^2$);
L = channel length (m);
$L_c$ = chord length;
$\mu$ = dynamic viscosity (Pa · s);
k = permeability (m$^2$);
$M_{x,y,z}$ = moment in x, y or z (N.m); and
M = Mach number (−).

### Definitions, acronyms and abbreviations

AoA = angle of attack;

© Ruan du Rand, Kevin Jamison and Barbara Huyssen. Published by Emerald Publishing Limited. This article is published under the Creative Commons Attribution (CC BY 4.0) licence. Anyone may reproduce, distribute, translate and create derivative works of this article (for both commercial and non-commercial purposes), subject to full attribution to the original publication and authors. The full terms of this licence may be seen at http://creativecommons.org/licences/by/4.0/legalcode

Special thanks are given to the National Integrated Cyber Infrastructure System (NICIS), Centre for High Performance Computing (CHPC) for the computational resources to conduct large cell Computational Fluid Dynamic (CFD) simulations in ANSYS Fluent.

The integration of the pod with the aircraft is funded by Armscor in terms of Order KT521936.

*Funding Statement:* The integration of the pod with the aircraft is funded by Armscor Order KT521936.

Received 9 October 2023
Revised 1 March 2024
1 May 2024
Accepted 30 May 2024

The current issue and full text archive of this journal is available on Emerald Insight at: **https://www.emerald.com/insight/1748-8842.htm**

Aircraft Engineering and Aerospace Technology
96/11 (2024) 10–18
Emerald Publishing Limited [ISSN 1748-8842]
[DOI 10.1108/AEAT-10-2023-0253]

CFD = computational fluid dynamics;
CG = Centre of gravity;
EM = electromagnetic;
FOV = field of view;
ISA = International Standard Atmosphere;
OEM = original equipment manufacturer; and
RANS = Reynolds averaged Navier–Stokes.

## Introduction

The integration of a new store onto an aircraft, especially for a large store, can be considered a major modification to the aircraft (Jamison and Heise, 2010). Integrating an electronics pod onto a high-performance jet aircraft is an airworthiness challenge, especially without the support of the aircraft's original equipment manufacturer (OEM). The lack of aircraft OEM support attracts significant scrutiny from the airworthiness certification authority, as no structural information about the aircraft and/or mounting pylon is available (Jamison, 2016).

The focus of this study is the second design iteration, Mk.2, of an electronics pod. The first design iteration, named Mk.1, presented several problems when its compatibility with the proposed carriage aircraft was investigated. The integration areas of concern were as follows:

- fitment clearance of the store on the aircraft and internal systems;
- loads on the aircraft during carriage; and
- impact on the aircraft's performance.

The MK.1 pod (Figure 1) consists of a cylindrical aluminium body with a blunt composite nose and tail cone. The pod also has box-shaped fairings protruding from the sides to house additional electronic components located far forward from the centre of gravity (CG). Three ram air inlets and outlets for internal cooling are situated in the nose and tail cones. The pod's mounting lugs are not positioned in the geometric centre of the pod and are slightly towards the back, giving the pod a longer overhang on the front with the fairings located far forward of the mounting position.

One method for certifying a store configuration when aircraft structural information is not available is through the method of analogy (Jamison, 2016) where the new store configuration is compared with stores that are already certified to the required operational loading (MIL-HDBK-1763, 1998). MIL-HDBK-1763 section 4.1.1 sets out the criteria for analogy that the "aerodynamic, structural, mass and operational characteristics of the store to be certified, are sufficiently similar to those of a store already certified in the desired loading configuration of the designated (or similar) aircraft". These criteria are not met for the Mk.1 pod investigated here.

**Figure 1** Electronics pod Mk. 1

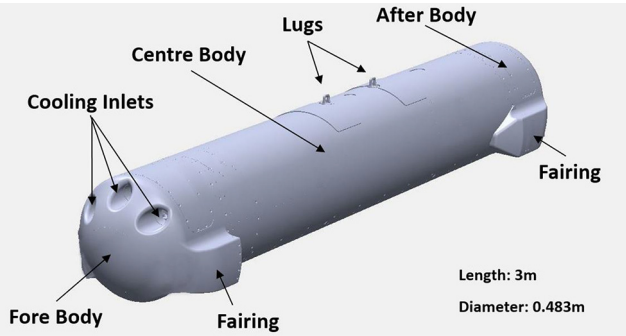


**Source:** Figure by authors

During carriage at Mach 0.75, the Mk.1 pod exceeds the known structural limits of the aircraft pylon by 14% in the axial force direction, 26% in the pitching moment axis and 80% in the yaw moment axis. Limiting the loads to the pylon's known limits reduces the aircraft velocity envelope by more than half while the aircraft's maximum G loading is restricted to less than a quarter of the full-load envelope. This reduction in the aircraft performance envelope was deemed unacceptable, and a redesign of the pod was required to maximise the flight envelope of the aircraft when carrying the pod.

The constraints on the external geometry of an electronics pod can be complex. For an electronics pod, the geometry not only affects the aeromechanical loads on the pod but also the electromagnetic (EM) performance. An emitting or receiving EM wave refracts and/or reflects when it passes through the radome medium (Dai *et al.*, 2021). The refractions and reflections increase as the angle of penetration between the EM wave and the radome increases. Electronic emitters and receivers therefore favour bluff aerodynamic geometries to reduce the amount of amplitude and phase corrections that must be made to the EM waves. In the Mk.1 pod aerodynamic performance was sacrificed for EM efficiency.

The blunter the bluff nose of a body in transonic flow becomes, the more rapidly the pressure coefficient located at the forebody shoulder increases (Coe and Kaskey, 1963). This large change in the pressure coefficient induces a reduction in the critical Mach number (where the airflow becomes locally supersonic) and generates a large flow separation bubble. The critical Mach number of Mk.1 pod was estimated to be ≈0.55.

Fairings housing EM sensors are placed on the sides of the pod. The fairings were located far forward from the CG in the Mk.1 pod to avoid contact with the undercarriage doors. Placing the fairings closer to the CG is undesirable as it positions the electronic receivers housed in the fairings underneath the wing, resulting in EM reflections from the wing to interfere with the electronic systems. The box-shaped fairings act as low-aspect-ratio wings that generate lift at non-zero Angles of Attack (AoA). The combination of the generated lift, longer moment arm and pressure drag generated excessive moments on the pylon at transonic velocities. The pod also suffers from a lack of passive drag and flow separation alleviation devices such as a boat tail afterbody.

Different methods can be used to determine the aeromechanical loads imposed by a new store on an aircraft's pylon, such as panel codes, computational fluid dynamics (CFD) software, wind tunnel tests and flight testing (NATO, 2014). The approach adopted in this case uses an empirical code, Missile DATCOM (Blake, 1998) to determine the initial pod fore-, centre- and afterbody configurations. Missile DATCOM version 1997 uses a semi-empirical datasheet component build-up method to analyse missile aerodynamics and performance. While it is not as accurate as computational aerodynamics codes, it is adequate for concept design and trade studies and its speed and ease of use enables the efficient exploration of a wide range of geometric configurations.

Once the main pod configuration is determined, the ARUV panel code (Jamison, 2018) is used to perform the initial analyses of the combined aircraft and pod configuration. Unlike the Missile DATCOM free stream analysis, the panel

code model the mutual aerodynamic interference between the aircraft and pod. ARUV is a low-order inviscid panel code with a fixed wake and several features supporting store carriage and separation analyses. It is a further development of the USTORE code (van den Broek, 1981) developed by the Council for Scientific and Industrial Research (CSIR). ARUV was also used to facilitate the design of fairings and stabilising fin configurations that were added to the main pod body to further improve the pod's compatibility.

The ARUV panel code does not model transonic flows or boundary layers and is thus not acceptable for verifying that the pod design complies with the aircraft load constraints. This was done using the Ansys CFD code. Before the final refinement was performed by CFD analysis, a validation study was performed to ensure that the complex flow field could be accurately modelled to represent the real flow field at a transonic velocity of Mach 0.75. A well-known carriage-and-store separation benchmark (Heim, 1990) for validation studies was used to validate the mesh, turbulence model and solver setup for the CFD analysis.

## Pod geometry constraints

One main cause for the inefficient design of the Mk.1 pod is due to the geometric constraints imposed on the pod. As stated in the previous section, the constraints are mostly due to the EM performance, as well as the existing mechanical components. The cylindrical centre body structure of the pod was repurposed from a different pod that was already structurally certified. The cylindrical centre body is the main structure of the pod where the mounting lug fittings and the internal system mounting fittings are, hence the structure may not be altered in any way. A ground vibration test and a flutter analysis had been conducted by the CSIR on the Mk.1 pod fitted to the carriage aircraft due to the large difference in pod size and mass compared with other store configurations on this aircraft. Thus, to remain within the scope of this flutter analysis; the mass of the improved pod design must be within 10% of the mass of the Mk.1 pod with the CG located in the same range.

The geometric constraints for the main body features are as follows:

- The existing cylindrical centre body of length 2 m and diameter of 0.483 m, remains unaltered;
- The forebody maximum fineness ratio of 1.5 (0.724 m) with a nose-tip fillet radius of 0.1 m;
- Afterbody maximum fineness ratio of 1.035 (0.5 m);
- Clearance tolerance of 0.01 m away from internal systems;
- The pod should be geometrically constrained to allow 1 inch (25.4 mm) of clearance from any surface on the carriage aircraft, excluding the mounting face of the pylon; and
- Must not impact the ground upon aircraft rotation or landing.

Additional constraints that are more design-specific are also implemented, such as respecting the field of view of the electronic receivers in the pod.

## Empirical and panel code analysis

The basic axial symmetric shapes of the fore, centre and afterbodies are designed first, as most of the aerodynamic loads are generated by these components owing to the large cross-sectional area. The geometries were initially designed in Missile DATCOM using free-stream conditions at the worst-case dynamic pressure condition [Mach number of 0.75 for International Standard Atmosphere (ISA) environmental conditions at sea level] for an angle of attack range of $-4° \leq \alpha \leq 4°$ in increments of 1°.

For the nose cone analysis, the afterbody is kept constant with an arc boattail at an angle of 12° that the effects of different nose geometry alternative can be compared. The different nose cone geometries that are considered, are all geometries that join tangentially to the shoulder of the centre body obtained from (Crowell, 1996). If the joint angle is not tangential, large pressure coefficient differences are generated at the shoulder and, even for a hemispherical forebody a critical Mach number of between 0.62 and 0.63 can be expected (Coe, 1961). Nose cones with longer fineness ratios (the ratio of the length of the nose to its maximum diameter) generally increase the critical Mach number.

The forebody geometries investigated using Missile DATCOM with an added nose fillet radius of 0.1 m are:

- Haack;
- Ogive;
- Karman; and
- Power Series ($n = 0.2, 0{,}5, 0.75$).

The afterbody's circular arc boat-tail geometry was analysed at a boat-tail angle of $8° \leq \beta \leq 14°$ in increments of 2°. The nose cone was kept constant to show only the effects of the boat-tail angle.

Figure 2 shows that all forebody configurations considered reduces the axial force ≈50% relative to the original Mk.1 pod geometry. The different forebody alternatives also reduce the pitching moment by ≈19% relative to the Mk.1 pod.

The afterbody's circular arc boattail geometry was evaluated for the following range of boattail angles: $8° \leq \beta \leq 14°$ in

**Figure 2** Nose cone geometries axial force coefficient (top) and pitching moment coefficient (bottom) M = 0.75

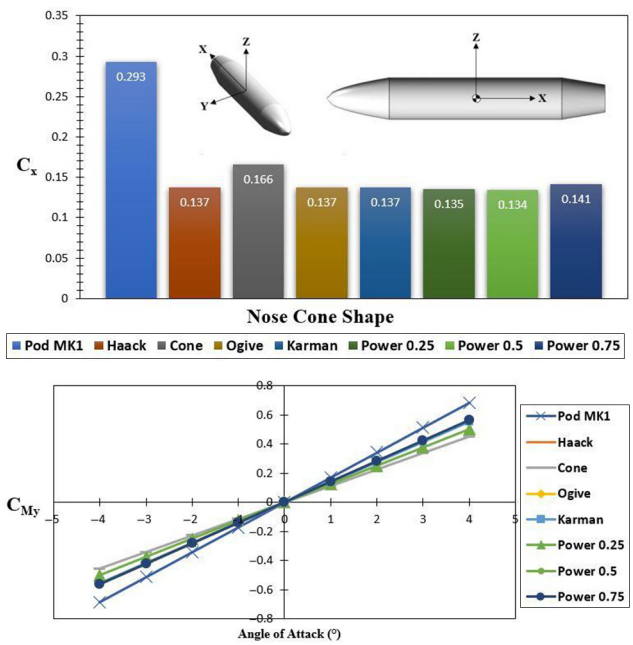


**Source:** Figure by authors

increments of 2°. The nose cone was kept constant to compare only the effects of the boattail angle. The Missile DATCOM results for boattail geometries show that, for the analysed range of boattail angles, the axial drag force decreases with a larger angle $\beta$. No difference was observed in the pitching moments between the afterbody configurations, indicating that the forebody was predominantly responsible for the pitching moment.

The final geometry selected the less optimal configuration of the Haack nose cone and 12° boattail due to constraints accommodating the pod's internal systems. The difference between the best and selected nose cone and boattail configurations is small, and both options result in a large overall aerodynamic improvement relative to the Mk.1 pod.

Fairings were added to the main body. Some of the pod's internal systems redistributed to enable the components housed in the fairings to be shifted inward, reducing total frontal cross-sectional area by 8.3% and the total fairing planform area by 53%

The ARUV panel code does not model internal flow of the pod's cooling system; thus, the ram air scoop is faired over as a protuberance. X-configuration stabilising fins were added to the boat tail section on the shoulder. This placement keeps the fins from interfering with the internal receivers and places the fins in the flow acceleration region of the afterbody, thereby maximising positive pressure gradients on the fins and the boattail. The airfoil section for the fin root is a 8% thick NASA supercritical section with a cord of 0.25 m and the tip airfoil is a 6% thick NASA supercritical section. The ram air scoop was placed on top of the nose cone forward of the nose cone/centre body junction.

When mounted on the carriage aircraft, the pod is pitched nose down by 1.43° on the pylon relative to the centreline of the aircraft. Even though the $x$-axis is aligned with the centreline of the pod, the free stream $\alpha$ is relative to the aircraft centreline, as the local $\alpha$ experienced by the pod is different owing to the mutual interference effect of the aircraft. The flight conditions are similar to the Missile DATCOM analysis free-stream conditions of ISA sea-level conditions at a Mach number of 0.75. The aircraft angle of attack ($\alpha$) and side-slip angle ($\beta$) were provided by the CSIR determined specific extreme manoeuvre cases of the flight envelope for the aircraft that would induce the largest force and moment loads on the pod. These load cases combine both inertial and aerodynamic loads.

To determine the acceptable load envelope for the pylon, the CSIR had computed loads imposed on the pylon by other stores certified by the OEM. These loads were used to define acceptable limit combinations of forces and moments at the ejector release unit on the pylon. An example is shown in (Figure 3) where the pylon acceptable limits are outlined in a

**Figure 3** Panel code moment load results M = 0.75

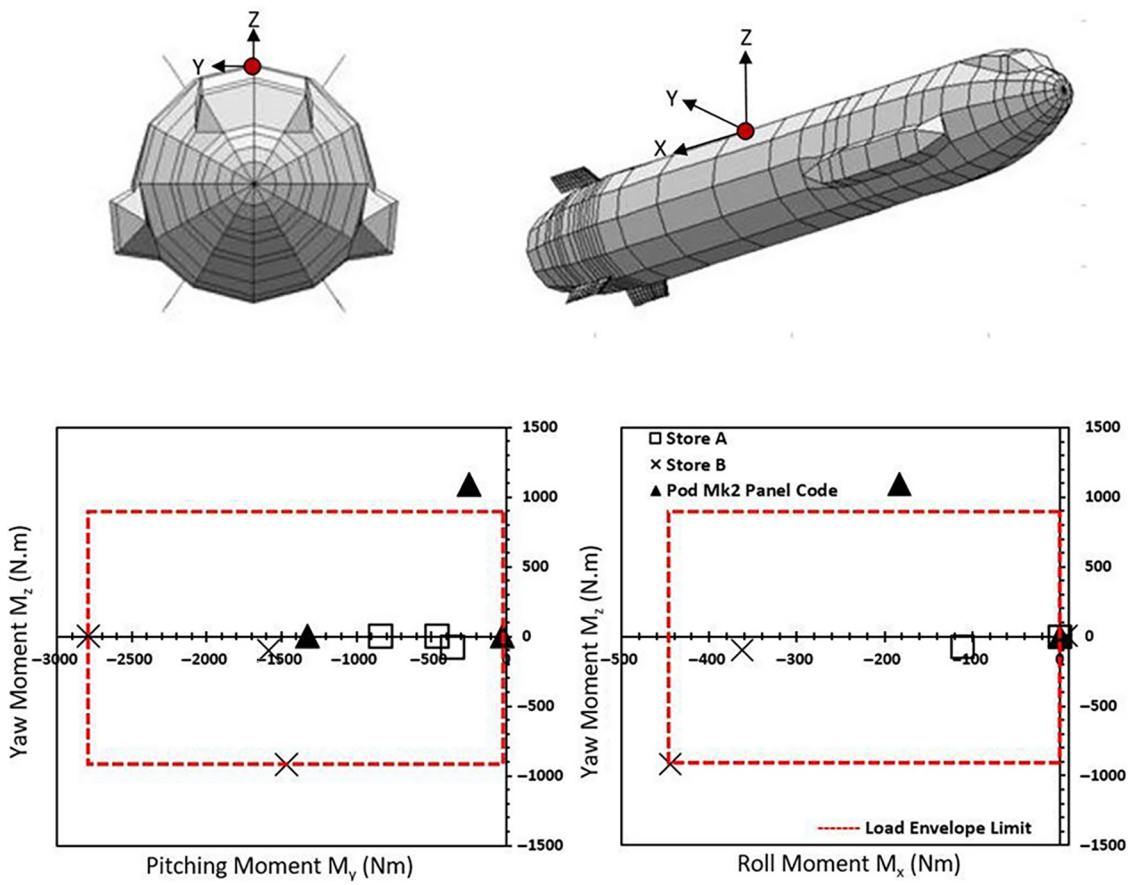


**Source:** Figure by authors

dashed red box. The initial panel code analysis results showed that the pod force loads were all within the load envelope but had a positive pitching moment $M_y$. As reference stores A and B only have negative pitching moments, the pod should have a negative pitching moment to comply with the analogy method, even if the positive moment is inside the structural limits of the aircraft. However, there is a lack of information to verify this. The stabilising fins are given a 2° nose up angle to provide the pod with a negative pitching moment. The yaw moment $M_z$ remains slightly outside the acceptable load envelope. The yaw moment was further investigated using a Reynolds Averaged Navier-Stokes (RANS) CFD analysis. Figure 3 shows the moment loads of the Mk.2 pod evaluated against the safe carriage load envelope of the aircraft pylon.

## Computational validation

The experimental case of (Heim, 1990) is widely used as a benchmark for transonic store carriage and separation validation data. The Heim experimental data is used in its carriage position on the pylon to validate the CFD approach used to analyse the pod on the pylon.

To encapsulate the model within the fluid domain, the recommended ANSYS Inc, 2009 Fluent user guide size is spherical with a diameter of 20 $L_c$. A quarter sphere was used to encapsulate the upstream domain and a half cylindrical body was used to encapsulate the downstream domain. The cylindrical body has a radius of 20 $L_c$. A secondary domain was added to capture the wake. The electronics pod has two exhaust outlets located on the end cap. Therefore, to capture the mixing of the exhaust with the external flow, this extra domain refinement zone is added in the validation case to examine whether it influences the force loads of the validation store.

Meshed using an unstructured grid with polyhedral elements, augmented by an inflation layer boundary to capture near-wall flow accurately. Turbulence models include k–$\omega$ SST, employing linear piecewise boundary layer inflation, and k–$\varepsilon$ with near-wall functions for boundary layer representation. A mesh-dependency study assessed cell size variation among turbulence models. For k–$\omega$ SST with a y+ value of 1 fully resolves viscous boundary layer with piecewise linear mesh step inflation. For k–$\varepsilon$, y+ value of 30 models wall in log-law region, resolving viscous sublayer with a wall function.

To study the differences between the two turbulence models, the pressure coefficients were plotted along specified locations on the store body and fins as a percentage of the distance along the cord or body length and then compared with the experimental results. The pressure coefficients of "body row 2" in Figure 4 are plotted alongside the experimental data.

There is a good correlation between the CFD results and experimental data. It was found that there is an almost negligible difference between the range of mesh sizes and turbulence models in the subsonic high-pressure regions located at the front of the various. The largest difference between the mesh sizes for each turbulence model is the prediction of the flow separation location at the rear of the components. These regions are heavily disturbed by transonic shock waves and shock reflections from neighbouring regions. It can be observed that the k–$\omega$ model is much more dependent on a finer mesh than the k–$\varepsilon$ model. For coarse k–$\omega$ meshes, flow separation occurs prematurely at 0.35 along the chord, as shown in Figure 4 for the $C_p$ location over the top surface of the wing.

The store is also evaluated alone at a free stream at a Mach number of 0.95 at an AoA range of 0° to 10° to validate the aeromechanical loads. A wall function and linear piecewise inflation boundary methods were evaluated for the k–$\omega$ SST models against a k–$\varepsilon$ wall function. Figure 4 shows the axial force coefficients ($C_x$) and pitching moment, including data from (Álvarez, 2022). A larger axial force coefficient could be contributed to the experimental setup of (Heim, 1990). The experimental model has no boundary layer tripping point, indicating that a large portion of laminar flow may be present around the store. However, the turbulent models used to numerically calculate the flow treat it as turbulent from the leading edge, causing the higher axial coefficients observed.

A larger difference was observed for the store pitching moment ($Cm_y$). The pressure-induced drag on the nose of the store dominates the pitching moment for the linear piecewise boundary layer, where the experimental data show that the stabilising fins should counteract the pitching moment (Figure 4). Even though at a larger angle of attack, the fins do indeed start counteracting the moment, and the angle of attack range of 1° to 8° is not modelled correctly. It was observed that the linear piecewise boundary layer is sensitive to the boundary layer mesh and could most likely yield more accurate results; however, it is a time-consuming task to determine the exact mesh cell size to model the flow correctly. The wall function method should be used as a good correlation between the experimental and CFD data is achieved.

## Computational simulation

The CFD analysis is computed using ANSYS Fluent 3D steady RANS solver. The fairing geometry and stabilising fins can now be optimised using this higher fidelity analysis tool. The fairing tips are elliptically shaped with a maximum allowable fineness ratio of 1.5 to avoid interfering with the pod's onboard receivers. Figure 5 shows the fairing tips parameterised in an asymmetric canting angle upward from 0° to 4°. This parametrisation was performed to determine whether the pressure distribution on the fairing tip could counteract the pitching moment of the pod.

The aircraft-pod configuration was meshed using an unstructured polyhedral mesh elements type to reduce the mesh cell count while maintaining the result accuracy (Spiegel *et al.*, 2011). To further reduce the number of meshing cells, the boundary layer is modelled in the log-law region using the "law of wall." This gives a $y^+$ value of 30 for the first cell layer height. The viscous sublayer was then modelled using a wall function rather than a linear piecewise function.

The effect of the internal flow of the cooling system was also modelled. Although it is not feasible to model the inside of the pod, as the intricate cooling system would most likely result in the same amount if not more computational resources than for the external flow. Therefore, a flow restriction model of the cooling system was incorporated into the pod modelling. The three ram air inlets and outlets were combined internally to

**Figure 4** Body (top left) and wing (top right) pressure coefficients, store axial (bottom left) and pitching moment (bottom right) coefficients, M = 0.95

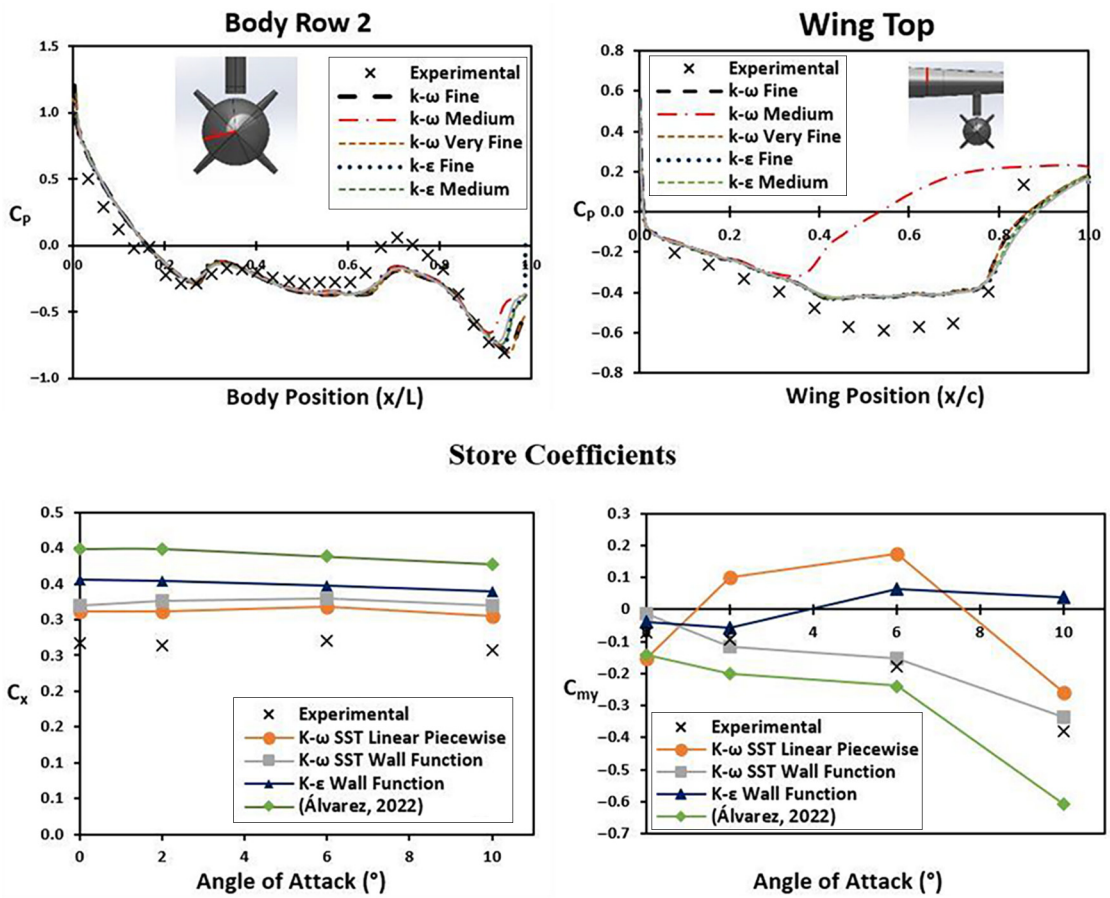


**Source:** Figure by authors

**Figure 5** Pod Mk.2 geometry and parameterisation

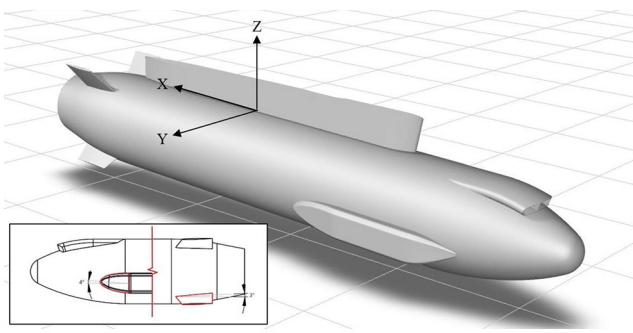


**Source:** Figure by authors

form a singular cylindrical channel. The cylindrical channel was modelled as a porous medium to simulate the flow friction pressure losses to the cooling system.

The designer of the cooling system provided the calculated pressure drop and volume flow through the cooling system under the flight conditions. To model a porous medium in ANSYS Fluent, the user input parameter for the flow resistance is the inverse of the permeability of the flow medium ($k^{-1}$):

Using Darcy's law (Knappett and Craig, 2012) of flow through a permeable medium, the permeability $k$ for the channel is determined by.

$$k = \frac{Q\mu L}{A\Delta p} \tag{1}$$

By inserting the client provided flow values into equation (2), the permeability k is determined to be.

$$k = 143.12\ x10^{-9} m^2$$

The initial results extraction found that an upwash on the afterbody for the "Pullout" and "Pushover" flight conditions negatively affected the bottom fins, which was not apparent in the panel code. The upwash generated a pitching moment on the bottom two fins that added to the pitching moment instability of the pod.

The pitching effect further increased due to the 2° nose-up cant angle on the fins introduced during the panel code analysis. An additional parameterisation of the bottom two fins is introduced, investigating canting the fins at a range of angles between −4° and 2° relative to the pod's centreline. By inverting the cant angle to −2° nose down, the desired stabilising effect is achieved with the fins producing a positive

pitching moment. The stabilising moment is increased with a cant angle of −4°, but the fins' induced drag increased with the increase in pitching moment. The fin cant angle was finalised at −3° nose down.

The total pitching moment was further reduced by increasing the nose-up cant angles at the front of the fairings. Although the reduction in the total moment was small, a reduction of 4.2% for an angle of 4° was still an improvement. The maximum fairing cant angle of 4° was used.

For the "Pullout" and "Rolling-Pullout" aircraft manoeuvre cases, no critical flow is present around the pod showing the pod is fully subsonic, but critical flow is seen in the "Pushover" case on the shoulders of the fairings (Figure 6). The maximum local Mach number is 1.018, indicating that the pod's carriage critical Mach number increased from ≈0.55 to ≈0.74. As the critical flow is low supersonic in a small region of the fairings, the wave drag is low and the drag divergence point was not reached in the aircraft's flight envelope.

When evaluating moment loads for the Mk. 2 pod against the load envelope box, a mixed set of results emerged, as shown in (Figure 7). In straight pull-out and pushover cases, the pitching moment, a primary concern, remained within load envelope limits. However, a notable issue arose during the "Rolling Pull-Out" flight condition. Both yaw and rolling moments exceeded the load envelope, with yaw moment surpassing by 78% and rolling moment by 16% (highlighted in green). The problem stems from the interplay between yaw and rolling moments, exacerbated by the negative $z$-axis positioning of fins in the axis system. Attempts to stabilise yaw moment ($M_z$) by increasing fin load lead to an undesirable rise in rolling moment ($M_x$), and vice versa. Adjusting fin body angle for yaw stabilisation poses clearance issues with lower fins and ground impact upon aircraft rotation. Placing upper fins in the wake of the pylon diminished their effectiveness. Consequently, the client approved a reduction in the aircraft's flight envelope on the roll axis, introducing a new "Rolling Pull-Out" manoeuvre condition to mitigate sideslip angle ($\beta$).

The upper fin span was increased to the maximum allowable limit, increasing the total planform area of the upper fins by 24%. The additional fin span above the pod centreline decreases the rolling moment $M_x$. With the increase in fin surface area and the minor flight envelope restriction, all force and moment coefficients fall within the allowable flight load envelope in Figure 7.

**Figure 6** Pod Mk. 2 "Pushover" flow field Mach number M = 0.75

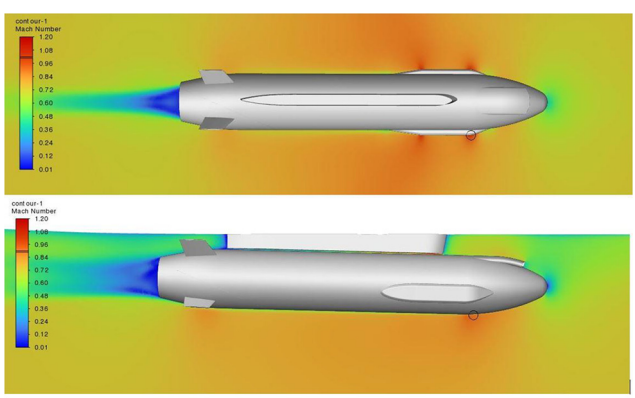


**Source:** Figure by authors

## Conclusion

The objective of recovering a fast-jet aircraft's flight envelope by redesigning an electronics pod to respect the structural load limitations is successful. The acceptable structural limits of the aircraft pylon were determined by analogy, where two reference stores, certified by OEM, are used to determine the pylon load limits. This proved to be a viable approach. The driving parameters for this study from the MIL-HDBK-1763 specification were the aircraft/store fitment, carriage loads and aircraft performance impact.

The pod's geometry was first established using Missile DATCOM, then further refined with the ARUV panel code. Due to loads nearing the aircraft's limits, ANSYS Fluent CFD analysis validated the results. CFD revealed the pod's mounting within the aircraft's boundary layer, leading to localised effects missed by inviscid panel code. Validation involved comparing CFD results with transonic experimental data, informing final adjustments to the pod design.

The redesign of the pod fully satisfied the geometric constraints set by the internal electronic components to reduce EM refraction and reflections. Interference with the undercarriage doors is averted by reducing the protrusion of the fairings from the main body, increasing the clearance to any part of the aircraft by more than 1 inch (25.4 mm). A boat tail afterbody was added to the back of the pod to ensure adequate ground clearance and reduce the base pressure drag.

Owing to the aerodynamic imbalance of the pod, due to the geometric constraints, the yaw and roll moments for a "Rolling Pull-Out" manoeuvre fell outside the load limits. Increasing the stabilizing fin area to counteract the yaw moment is not possible because the yaw and rolling moments adversely affect each other. By restricting the aircraft's roll rate, the side-slip angle ($\beta$) at the pod for this manoeuvre was reduced by 45%. This reduction in $\beta$ reduces the yaw and roll moments to within the safe carriage load envelope.

Re-lofting the pod geometry increased the carriage critical Mach number of the pod ≈0.55 to ≈0.74. The total axial force load for the Mk.2 pod was reduced by 61.6%. This is due to the combination of reduced pressure and wave drag, as well as the elimination of significant regions of flow separation. The goal of retaining the full manoeuvre envelope of the aircraft when integrated with the pod was mostly achieved, with only a roll-rate restriction being required.

This study emphasizes the importance of optimising store design within the carriage environment to enhance aircraft/store performance. It highlights the limitations of relying solely on inviscid codes, especially for determining carriage loads on fuselage-mounted stores where boundary layer effects are significant. In such cases, employing CFD codes, despite higher computational costs, is justified for accurate assessments.

**Figure 7** Moment loads of Mk.2 pod compared to reference stores and Mk.1 pod for the unrestricted (top) and restricted (bottom) aircraft manoeuvre envelopes M = 0.75

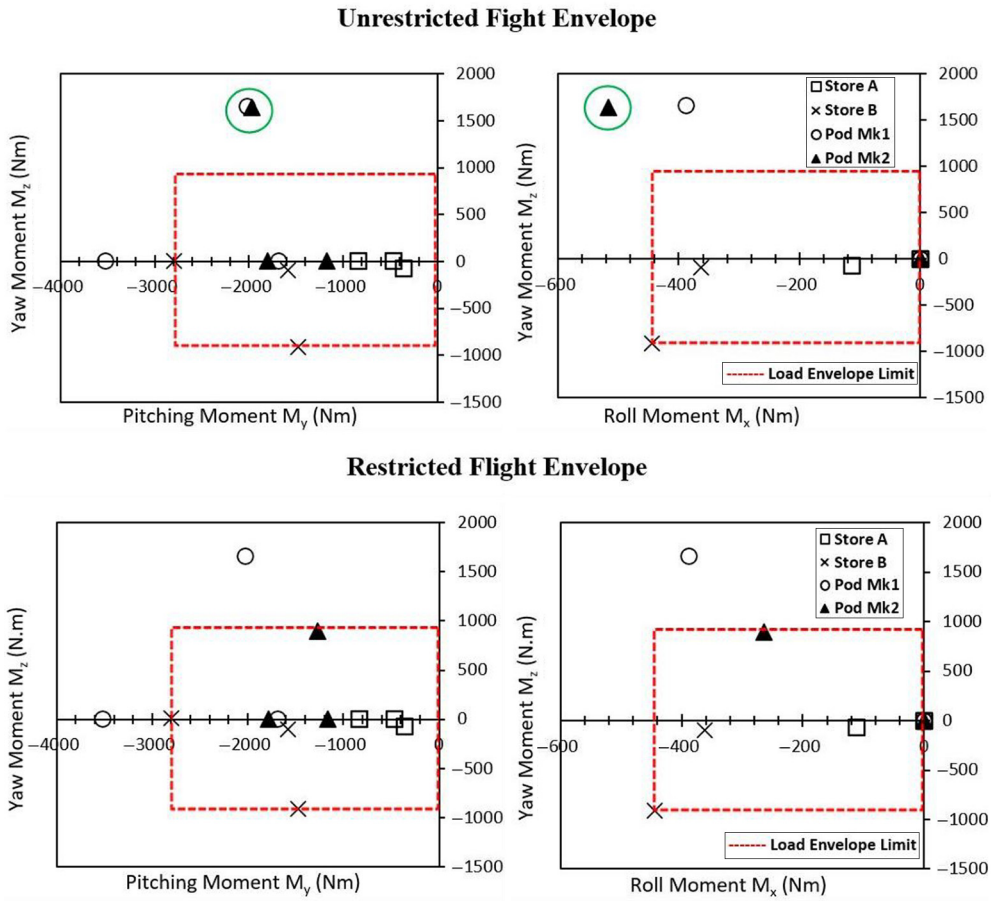


**Source:** Figure by authors

## References

Álvarez, J.I.R. (2022), "Transonic CFD analysis of an external store carried on a military aircraft wing", *Dpto. Ingeniería Aeroespacial y Mecánica de Fluidos Escuela Técnica Superior de Ingeniería*, Universidad de Sevilla, Sevilla.

ANSYS Inc (2009), "Porous media conditions", available at: https://www.afs.enea.it/project/neptunius/docs/fluent/html/ug/node233.html (accessed 10 August 2022).

Blake, W.B. (1998), *Missile DATCOM: User's Manual—1997 Fortran 90 Revision*, U.S. Air Force Research Lab./Air Vehicles Directorate, Wright–Patterson AFB, OH.

Coe, C.F. (1961), *Steady and Speeds on Fluctuating Pressures at Transonic Two Space-Vehicle Payload Shapes*, NASA, Ames Research Centre Moffett Field, Calif.

Coe, C.F. and Kaskey, A.J. (1963), *The Effects of Nose Bluntness on the Pressure Fluctuations Measured on 15' and 20' Cone-Cylinders at Transonic*, NASA, Ames R e s e a r c h C e n t re Moffett Field, Calif.

Crowell, G.A. Sr. (1996), "The descriptive geometry of nose cones", available at: https://dokumen.tips/documents/the-descriptive-geometry-of-nose-cone.html (accessed 8 June 2021).

Dai, L., Xie, Y., Zhang, C. and Wu, P. (2021), "Fast optimization of array antenna enclosed by asymmetric radome using AEP combined with enhanced HGAPSO", *Progress In Electromagnetics Research M*, Vol. 103, pp. 161-171.

Heim, E.R. (1990), *CFD Wing/Pylon/Finned Store Mutual Interference Wind Tunnel Experiment*, Arnold Engineering Development Center, Arnold Air Force Base, TN, Air Force Systems Command, United States Air Force.

Jamison, K.A. (2016), *Using the Similarity Argument to Integrate Stores with Aircraft: Two Case Studies with Electronic Pods*, International Aerospace Symposium of South Africa,. Pretoria.

Jamison, K.A. (2018), "Grid-mode transonic store separation analyses using modern design of experiments", 31st Congress of the International Council of the Aerospace Sciences. *Belo Horizonte*.

Jamison, K.A. and Heise, R. (2010), *Evaluating the Release of a Large Store from the BAE Hawk Mk120*, International Aerospace Symposium of South Africa, Gordon's Bay.

Knappett, J.A. and Craig, J.F. (2012), "Craig's soil mechanics", 8th ed, *2 Park Square*, Spon Press, Milton Park, Abingdon, Oxon OX14 4RN.

MIL-HDBK-1763 (1998), "Aircraft/stores compatibility: systems engineering data requirements and test procedures", available at: http://everyspec.com/MIL-HDBK/MIL-

HDBK-1500-1799/MIL_HDBK_1763_1775/ (accessed 4 April 2021).

NATO (2014), "Aircraft/stores compatibility, integration and separation testing", *Science and Technology Organization North Atlantic Treaty Organization BP 25*, F-92201 Neuilly-sur-Seine Cedex.

Spiegel, M., Redel, T., Zhang, Y.J., Struffert, T., Hornegge, J., Grossman, R.G., Doerfler, A. and Karmonik, C. (2011), "Tetrahedral vs. polyhedral mesh size evaluation on flow velocity and wall shear stress for cerebral hemodynamic simulation", *Computer Methods in Biomechanics and Biomedical Engineering*, Vol. 14 No. 1, pp. 9-22.

Van Den Broek, G.J. (1981), "The analytical prediction of the separation behaviour of external stores after release from the carrier aircraft", D. Eng. Thesis, University of Pretoria, South Africa.

## Further reading

Compton, W.B. (1968), "Effect on base drag of recessing the bases of conical afterbodies at subsonic and transonic speeds", *National Aeronautics and Space Administration*, Washington, DC, Washington, DC, NASA TN D-4821.

Heim, E.R. (1991), *CFD Wing/Pylon/Finned Store Mutual Interference Wind Tunnel Experiment*, AEDC-TSR-91-P4, USAF Arnold Engineering Development Center.

## Corresponding author

**Ruan du Rand** can be contacted at: u15013962@tuks.co.za

For instructions on how to order reprints of this article, please visit our website:
**www.emeraldgrouppublishing.com/licensing/reprints.htm**
Or contact us for further details: **permissions@emeraldinsight.com**